Electrografting of mixed organophosphonic monolayers for SI-ATRP of 2-methacryloyloxyethyl phosphorylcholine

Bastien Arrotin, Jean-Marc Noël, Joseph Delhalle, Laetitia Mespouille, Zineb Mekhalif

Electrografting of mixed organophosphonic monolayers for SI-ATRP of 2-methacryloyloxyethyl phosphorylcholine

Bastien Arrotin , Jean-Marc Noël, Joseph Delhalle, Laetitia Mespouille, Zineb Mekhalif

Abstract Nitinol (NiTi), one of the most important alloys for biomedical applications, is still hampered by its surface nickel inclusions, making it sensitive to pitting corrosion and leading therefore to the release of potentially carcinogenic Ni^{2+} ions. In this work, we assess the impact of the combination of electrografted mixed self-assembled monolayers (SAMs) on NiTi followed by a polymer coating formed by surface-initiated atom transfer radical polymerization (SI-ATRP). The molecular ratio of 11-(2-bromoisobutyrate)-undecyl-1-phosphonic acid (BUPA) to 11-decylphosphonic acid ($C_{10}P$) on the electroassisted elaboration of the (BUPA/$C_{10}P$)-NiTi-SAMs has been optimized. A small amount of BUPA (20%) appears to be the most promising condition, as it provides an efficient corrosion resistance and promotes the SI-ATRP of 2-methacryloyloxyethyl methacrylate (MPC). This confers to the surface hydrophilic properties and corrosion resistance close to those NiTi-SAMs when long polymerization times are used (≥ 6 h).

Graphical abstract

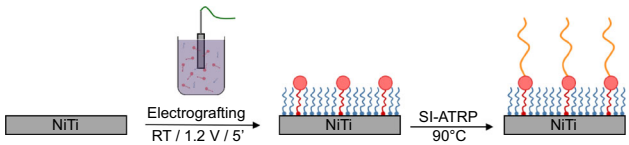

Keywords Nitinol, Organophosphonic acids self-assembled monolayers (SAMs), Electroassisted grafting, SI-ATRP, Corrosion, MPC polymer coating

Electronic supplementary material The online version of this article (https://doi.org/10.1007/s11998-019-00186-6) contains supplementary material, which is available to authorized users.

B. Arrotin, J. Delhalle, Z. Mekhalif (✉)
Laboratory of Chemistry and Electrochemistry of Surfaces (CES), University of Namur, rue de Bruxelles, 61, 5000 Namur, Belgium
e-mail: zineb.mekhalif@unamur.be

B. Arrotin
e-mail: bastien.arrotin@unamur.bebastien.arrotin@umons.ac.be

J. Delhalle
e-mail: joseph.delhalle@unamur.be

B. Arrotin, L. Mespouille
Laboratory of Polymeric and Composite Materials (LPCM), Center of Innovation and Research in Materials and Polymers (CIRMAP), HEALTH and MATERIALS Research Institutes, University of Mons, Place du Parc, 23, 7000 Mons, Belgium
e-mail: laetitia.mespouille@umons.ac.be

J.-M. Noël
Université Paris Diderot, ITODYS, CNRS, UMR 7086, Université Sorbonne Paris Cité, 15 rue J. de Baïf, 75013 Paris, France
e-mail: jean-marc.noel@univ-paris-diderot.fr

Introduction

Nitinol, a nearly equiatomic nickel titanium alloy, has a number of interesting intrinsic properties including heat, impact and corrosion resistance, high fatigue strength,[1,2] super-elasticity close to that of bone[3] and shape memory.[4–6] This makes NiTi applicable in a wide range of biomedical materials such as self-expending stents, surgical endoscopic instruments, atrial septal occlusion devices, orthodontic wires, and orthopedic staples and plates.[7–10] The major limitation of untreated NiTi is the risk of corrosion due to its oxide breakdown. Although the TiO_2 surface layer is spontaneously formed and highly contributes to its corrosion protection,[11] the remaining nickel inclusions

in the superficial layer can induce NiTi pitting corrosion[12–14] and lead to the release of Ni^{2+} ions into bodily fluids. This generates allergenic and inflammatory reactions, breathing problems, or even various cancers such as lung, kidney, or liver.[15,16] Various processes have been developed for NiTi surface modification to enhance its corrosion resistance and confer other interfacial properties such as wettability, protein absorption prevention, biocompatibility, and/or bioactivity increase. Among them, plasma treatment,[17–19] chemical vapor deposition,[20,21] hydrothermal reinforcement of the oxide layer,[22,23] self-assembled monolayers (SAMs),[24–26] and surface initiation of polymers[23,27] have been reported.

In the present work, we combine the last two processes to modify NiTi surfaces. SAMs based on organophosphonic acid derivatives are selected because they are known to robustly graft on metal oxide surfaces via M–O–P bonds which are very resistant to hydrolysis.[28–32] They constitute a strong reinforcement of the metal surface in aggressive environments.[33–37] To confer to the surface additional properties for applications, e.g., antifouling,[38,39] lubrication,[40,41] cell culture[42,43] or even cell differentiation,[44] appropriate polymer coatings are also used. One way to generate theses polymers is the surface-initiated controlled radical polymerization (SI-ATRP) which leads to the growth of polymer brushes with a good level of control over chain length, grafting density, and molecular architecture.[39,45–47]

ATRP mechanism is based on the reversible catalyzed homolytic rupture of the alkyl–halogen bond of the initiating group (e.g., bromoisobutyrate). The relative weakness of the C–Br bond (E_b = 318.0 ± 8.4 kJ mol^{-1}),[48] unstable in certain surface treatment conditions such as induction heating,[49] decreases the efficiency of SI-ATRP. The electroassisted approach, recently reported for Ti–6Al–4V[50] and NiTi,[49,51] has considerable advantages to lead to the formation of high-quality SAMs within short modification times and at room temperature. Thus, it is an alternative way to graft SI-ATRP initiators based on phosphonic acid derivatives while preserving the sensitive chemical functions, such as C–Br in the 11-(2-bromoisobutyrate)-undecyl-1-phosphonic acid (BUPA) used as ATRP initiator.[49] However, BUPA initiating functions are quite bulky and may lead to disordered and less protective layers. The use of mixed monolayers resulting from the co-adsorption of two organophosphonic acid derivatives differing in length and/or terminal functional groups has been reported to improve the corrosion resistance as well as the layer organization.[47,52–54]

Among the promising and versatile surface characterization techniques, scanning electrochemical microscopy (SECM), based on the use of an ultramicroelectrode facing a substrate, allows the local probing of its electrochemical property, i.e., its conducting/insulating behavior, and can provide high-resolution information on the electrochemical processes occurring at the surface.[55–58] Over the last years, SECM has been widely applied for the study of self-assembled monolayer properties and impact over corrosion resistance[26,59–61] and on organic layer permeability.[62] But so far, only few SECM studies have been performed on Nitinol,[26] which thus remains of great interest.

The aim of this work is to improve the quality of the electrografted SAMs on NiTi. To this end, mixed SAMs carrying alkyl-halogen initiating groups of 11-(2-bromoisobutyrate)-undecyl-1-phosphonic acid (BUPA) are formed on NiTi after its hydrothermal treatment by incorporating 1-decylphosphonic acid ($C_{10}P$) molecules with a shorter hydrophobic alkyl chain. Various amounts of BUPA/$C_{10}P$ are studied to optimize the quality of the SAM organization and consequently the NiTi corrosion resistance while keeping sufficient amount of grafted BUPA for the polymerization. The so-formed mixed SAMs are used to initiate the surface polymerization of 2-methacryloyloxyethyl phosphorylcholine (MPC), a biocompatible monomer (Scheme 1). The originality of this work resides in the combination of the electroassisted approach for the grafting of mixed monolayer which is in itself a relatively new promising method and is particularly suitable for temperature-sensitive groups. In this context, the SI-ATRP can be considered as an indirect evaluation way for the achievement of those surface modifications. The benefits of this method are highlighted over NiTi corrosion inhibition, surface functionalization and physicochemical properties.

Experimental section

Chemicals

Disolol® (ethanol 99% denatured with isopropanol 2% and Butanone 2%, ChemLab), 11-(2-bromoisobutyrate)-undecyl-1-phosphonic acid (BUPA, Sikémia, ≥ 97%), 1-decylphosphonic acid ($C_{10}P$, abcr, 98%), tris[2-(dimethylamino)ethyl]amine (Me_6TREN, Aldrich, 97%), potassium nitrate (Merck, 98%), ferrocenemethanol (FcMeOH, Aldrich, 97%), and sodium chloride (Fluka, ≥ 99.5%) are used without further purification. 2-Methacryloyloxyethyl phosphorylcholine (MPC) (Sigma-Aldrich, 97%) is purified from the remaining stabilizing agent by mixing it with anhydrous diethyl ether and filtering.[55] Copper(I) bromide (Aldrich, 99%) is purified by consecutive washings with acetic acid and methanol and finally maintained under N_2 atmosphere. All aqueous solutions are prepared with ultrapure Milli-Q water (18.2 MΩ cm).

Nitinol substrates preparation

Nitinol (Ni 56%/Ti 44%) rectangular-shaped plates (20 mm × 10 mm × 0.3 mm), purchased from AMF,

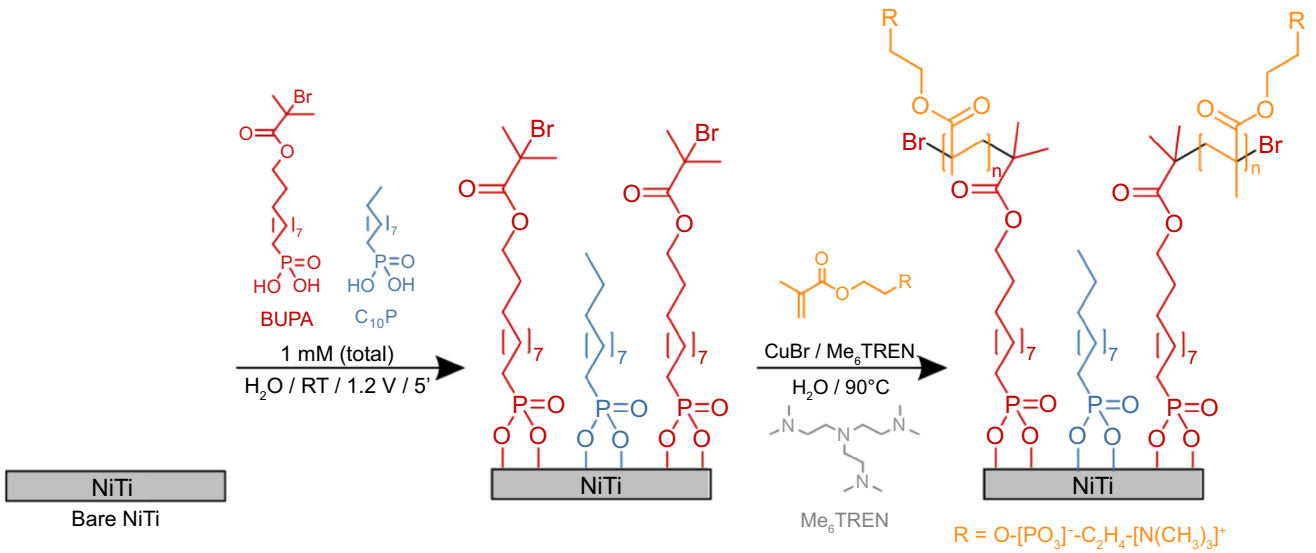

Scheme 1: Surface modification of Nitinol: self-assembly of BUPA/C_{10}P mixed monolayers (left) and subsequent SI-ATRP of MPC in the presence of Me_6TREN (right)

are mechanically polished down to 0.1 μm roughness on a Buehler Ecomet 300 instrument using silicon carbide papers, diamond pastes (9 μm) from Struers, and a mixture of colloidal silica (Buehler MasterMet^{TM} 2) and H_2O_2 (Acros Organics, 35 wt% solution in water). These Nitinol substrates (subsequently denominated bare NiTi) are cleaned in denatured ethanol under ultrasonication for 15 min before being blown dry with nitrogen and stored under nitrogen for further use or analysis.

Prior to any modification, the substrates are systematically cleaned by application of the following treatments: immersion in denatured ethanol in a sonication bath for 15 min, drying under nitrogen, hydrothermal treatment in boiling water for 1 h (HT-NiTi), and finally cleaning in denatured ethanol for 15 min under sonication, before being blown dry under nitrogen.

Electroassisted grafting of mixed initiating monolayers on Nitinol

Solutions (20.0 mL) composed of 1 mM of a mixture of 11-(2-bromoisobutyrate)-undecyl-1-phosphonic acid (BUPA)/1-decylphosphonic acid ($C_{10}P$) in various ratios and 10 mM KNO_3 are prepared in ultrapure Milli-Q water.

The SAMs on HT-NiTi surface are obtained by immersion of the substrate in the solution for 5 min, under a voltage of 1.2 V vs a saturated calomel electrode (SCE) using a Princeton Applied Research VersaSTAT3 potentiostat/galvanostat. At the end, the substrates are ultrasonically cleaned in denatured ethanol for 15 min, before being blown dry under nitrogen and stored for characterizations.

SI-ATRP of MPC

To a four-neck round-bottomed flask are added 3.0×10^{-4} mol copper bromine (CuBr) and 6.0×10^{-4} mol tris[2-(dimethylamino)ethyl]amine (Me_6TREN). The three lateral necks are closed by septa into which a clip is inserted to hold two substrates. The flask is then purged by three repeated vacuum/nitrogen cycles. In a second round-bottomed flask are introduced 3.4×10^{-3} mol of 2-methacryloyloxyethyl phosphorylcholine and 19.8 mL of Milli-Q water to reach a concentration of 0.17 M. The solution is then deaerated by nitrogen bubbling for a few minutes.

The content of the second flask is transferred into the first one by means of a flamed dry capillary under N_2 atmosphere. The polymerization is then carried out for 1, 3, or 6 h at 90°C in an oil bath. At the end of the reaction, the flask is cooled down to room temperature. The substrates are then rinsed with denatured EtOH and sonicated in denatured EtOH for 15 min. They are finally dried and stored under N_2 atmosphere.

Substrate characterization

The modified substrates are characterized by X-ray photoelectron spectroscopy (XPS), polarization modulation-infrared reflection–absorption spectroscopy (PM-IRRAS), static water contact angle measurements (WCA), cyclic voltammetry (CV), linear sweep voltammetry (LSV), and scanning electrochemical microscopy (SECM). To assess the reproducibility of the grafting, all the analyses were performed in triplicate. In the case of XPS characterizations, each sample is analyzed at three different spots.

XPS spectra are recorded on a Thermo Scientific K-Alpha spectrometer using a monochromatized X-ray K_α radiation (1486.6 eV), the photoelectrons being collected at 0° with respect to the surface normal and detected with a hemispherical analyzer. The spot size of the X-ray source on the sample is 200 μm, and the analyzer is operated with a pass energy of 200 eV for survey spectra and 50 eV for high-resolution core-level spectra. The binding energy (BE) of core levels is calibrated with respect to the C1s BE set at 285.0 eV. Spectra are analyzed using a linear combination of Gaussian and Lorentzian curves in 70–30 proportions. The different relative peak areas are measured on core-level spectra. Quantitative XPS analyses are carried out by calculating the relevant abundance ratios on the basis of the core-level spectra and taking into account the corresponding Scofield sensitivity factors[56]: C1s 1.000, P2p 1.920, N1s 1.800, Ti2p 7.910, and Ni2p 22.180. Thickness of the formed coatings is estimated from the collected XPS data. The thickness of a first material (i.e., SAM) deposited on a bulk material (i.e., NiTi) can be obtained from the relative attenuation of this bulk material (here limited to Ti), by the formula:

$$\frac{I_{\mathrm{Ti}}}{I_{\mathrm{Ti},0}} = \exp\left(-\frac{d_{\mathrm{SAM}}}{\lambda_{\mathrm{Ti,SAM}}}\sin\theta\right) \quad (1)$$

where $I_{\mathrm{Ti}}/I_{\mathrm{Ti},0}$ is the ratio of the bulk element peak intensities (modified/bare surface), d_{SAM} the coating thickness, $\lambda_{\mathrm{Ti,SAM}}$ the bulk Ti photoelectrons mean free path through the SAM layer, and θ the takeoff angle (here $\theta = 90°$).[57–59]

PM-IRRAS data are collected to assess the presence of the organic layer on nickel surfaces. They are recorded on a Bruker PMA37 equipped with a liquid nitrogen-cooled mercury–cadmium–telluride (MCT) detector and a germanium crystal. All presented spectra are the average of 1024 scans at a spectral resolution of 4 cm^{-1}.

Static water contact angle measurements are carried out using a DIGIDROP (GBX Surface Technology) goniometer at room temperature and ambient atmosphere, with a syringe to deliver 2 μL droplet of Milli-Q water.

Voltammetry measurements (CV and LSV) are carried out on a Princeton Applied Research, Potentiostat/Galvanostat Model VersaSTAT3-LC using a three-electrode electrochemical cell with a controlled analysis spot surface (0.28 cm^2) on the sample. Nitinol substrates (bare or modified) are used as working electrode, a platinum foil as counter electrode, and a saturated calomel electrode (SCE) as reference.

Cyclic voltammograms are recorded from − 0.10 to + 0.65 V at a scan rate of 20 mV s^{-1} in 0.1 M NaOH. The blocking factor (BF) of the coatings on NiTi is determined from the formula:

$$\mathrm{BF} = \frac{a_{\mathrm{an},0} - a_{\mathrm{an}}}{a_{\mathrm{an},0}} \times 100 \quad (2)$$

where $a_{\mathrm{an},0}$ and a_{an} are the area of the anodic peaks for the first cycle of bare and modified NiTi substrates, respectively.

Linear sweep voltammograms are recorded from 200 mV below OCP (measured for 1 h) to + 1.0 V at a scan rate of 1 mV/s in 0.5 M NaCl. The corrosion inhibition efficiency (IE) is determined from the obtained corrosion current densities (j_{corr}) by the formula:

$$\mathrm{IE} = \frac{j_{\mathrm{corr},0} - j_{\mathrm{corr}}}{j_{\mathrm{corr},0}} \times 100 \quad (3)$$

where $j_{\mathrm{corr},0}$ and j_{corr} are the corrosion current densities of bare and modified NiTi substrates, respectively.

SECM is operated in a feedback (FB) mode on a CHI 900B Bi-potentiostat (CH Instruments) using a three-electrode cell: a commercial Ag|AgCl reference electrode (CHI111, CH Instruments), a platinum foil as counter electrode, a platinum microdisc ultramicroelectrode (UME) (10 μm diameter with an estimated RG ratio of 8). The sample is fixed at the bottom of the cell without polarization. FB mode analyses were performed in a 1 mM FcMeOH/0.1 M KNO_3 aqueous solution according to the following procedure. The UME is polarized at 0.40 V vs Ag|AgCl to allow the mass-transfer-controlled oxidation of FcMeOH to ferricenium methanol ($FcMeOH^+$) and moved down toward the substrate at a rate of 1 μm s^{-1}. The approach curve is recorded until a sharp change of the currents occurred at the tip. The UME is then withdrawn by 3 μm, and the imaging measurements is taken on a 500 × 500 μm^2 area at a scan rate of 25 μm s^{-1}.

Results and discussion

The results are presented in two sections: the first one deals with the NiTi modification with phosphonic acid derivatives based on $C_{10}P$, BUPA, or mixtures of BUPA/$C_{10}P$ molecules in different proportions to achieve monolayers in order to confer to NiTi multifunctional properties such as corrosion protection and the ability to initiate SI-ATRP. The second part deals with the benefit of using modified NiTi with mixed BUPA/$C_{10}P$ SAMs on the SI-ATRP of MPC, a model of biocompatible monomer.

Electroassisted grafting BUPA/$C_{10}P$ mixed monolayers

The electroassisted approach, based on the optimized conditions determined in our previous work (E = 1.2 V vs SCE and t = 5 min),[49] is transposed to the grafting of $C_{10}P$ ($C_{10}P$-NiTi), BUPA (BUPA-NiTi), and their mixture in different ratios (BUPA/

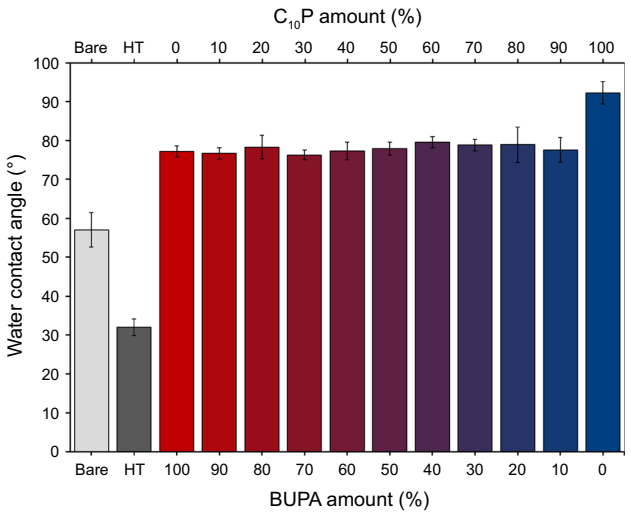

Fig. 1: Water contact angles for bare NiTi, HT-NiTi, BUPA-NiTi, C_{10}P-NiTi, and BUPA/C_{10}P-NiTi (in various ratios)

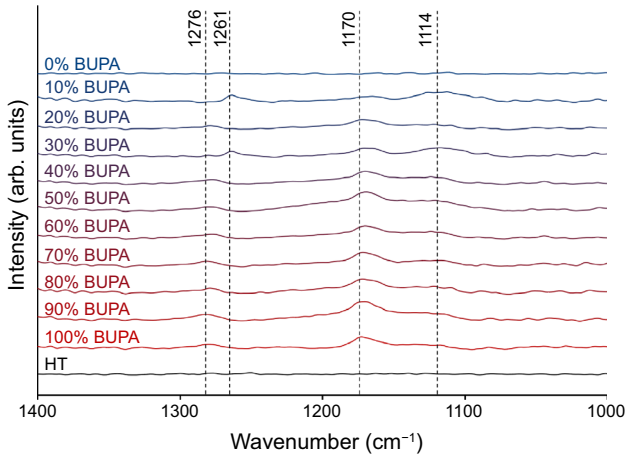

Fig. 2: PM-IRRAS spectra for HT-NiTi, BUPA-NiTi, C_{10}P-NiTi, and BUPA/C_{10}P-NiTi (in various ratios)

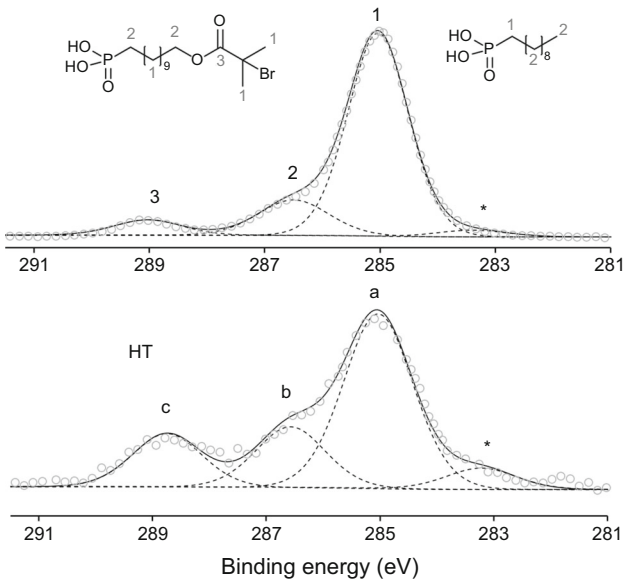

Fig. 3: Representative XPS C1 s core levels for HT-NiTi (bottom) and BUPA/C_{10}P-NiTi in various ratios (top)

C_{10}P-NiTi) on HT-NiTi. The resulting modified NiTi surfaces are characterized with contact angle measurements, PM-IRRAS, XPS, and electrochemical analyses.

Figure 1 highlights the wettability properties of bare NiTi, HT-NiTi, C10P-NiTi, BUPA-NiTi, and BUPA/C_{10}P-NiTi. The water contact angle values (θ_w) ranging from 78° to 92° after NiTi modification point to a significant increase in the contact angle compared to HT-NiTi (θ_w = 30°). The highest θ_w value, indicating the more hydrophobic surface, is obtained for C_{10}P-NiTi (θ_w = 92°). Increasing the ratio of BUPA/C_{10}P does not drastically change the θ_w values which remain very close ($\theta_w \sim 80°$) to that of BUPA-NiTi. This is consistent with the fact that C_{10}P molecules are shorter than BUPA and thus have less impact on the wettability properties, even at high concentration in the mixed monolayer.

Figure 2 displays PM-IRRAS spectra for HT-NiTi and BUPA/C_{10}P-NiTi. HT-NiTi does not show any signal of any chemical functions, while BUPA/C_{10}P-NiTi show, whatever the molecular ratio, vibrational bands typical of BUPA at 1276/1261 and 1170 cm^{-1}, assigned, respectively, to the asymmetric and the symmetric stretching of the C–O bond of the bromoisobutyrate function, and to C–H deformation.[60]

Results of the X-ray photoelectron spectroscopy (XPS) analyses performed on HT-NiTi and modified NiTi are reported in Fig. 3 and Table 1. C1s core level (Fig. 3) displays peaks at similar energies but with higher intensities for modified NiTi indicating therefore an effective grafting of C_{10}P and BUPA on HT-NiTi. These peaks at energies of 285 eV, 286.5 eV, and 289.1 eV, correspond, respectively, to carbon atoms involved in C–H/C–C, C–O/C–P, and O–C=O bonds present in the phosphonic acid derivatives (peak 1 for C_{10}P) and (peaks 1–3 for BUPA) or in atmospheric contaminations (peaks a-c for HT-NiTi). The one at 283.3 eV (*) is assigned to an artifact from the spectrometer.

In addition to the increase in C1s intensity, XPS analyses reveal the presence of P2p for all BUPA-NiTi, C_{10}P-NiTi and BUPA/C_{10}P-NiTi and Br3 s for BUPA-NiTi and BUPA/C_{10}P-NiTi. When adding C_{10}P to BUPA, the C/NiTi and P/NiTi ratios increase (Table 1) indicating the formation of denser and more organized layers due to the insertion of C_{10}P. The maximum is achieved for 60% of BUPA. The C/NiTi ratio then decreases due to the shorter chain of C_{10}P replacing the longer BUPA ones while P/NiTi remains almost stable (0.13–0.17). The Br/NiTi ratio is barely affected by the decrease in BUPA amount which proves that pure BUPA layer is not very well organized and partially degraded.

Table 1: XPS atomic ratios for bare NiTi, HT-NiTi, and (BUPA/C_{10}P)-NiTi (various ratios) and estimated SAM thickness

Sample	C/NiTi	P/NiTi	Br/P	d_{SAM} (nm)
Bare	0.30 ± 0.10	–	–	–
HT	0.10 ± 0.20	–	–	–
100% BUPA	1.03 ± 0.32	0.09 ± 0.01	0.23 ± 0.05	1.93 ± 0.38
90% BUPA	1.34 ± 0.48	0.11 ± 0.01	0.23 ± 0.07	1.90 ± 0.15
80% BUPA	1.63 ± 0.27	0.11 ± 0.01	0.25 ± 0.05	1.83 ± 0.15
70% BUPA	2.29 ± 0.23	0.15 ± 0.01	0.21 ± 0.02	1.87 ± 0.15
60% BUPA	2.51 ± 0.25	0.17 ± 0.01	0.18 ± 0.01	1.71 ± 0.12
50% BUPA	1.93 ± 0.20	0.15 ± 0.01	0.18 ± 0.02	1.76 ± 0.16
40% BUPA	1.64 ± 0.10	0.13 ± 0.01	0.16 ± 0.02	1.58 ± 0.07
30% BUPA	1.68 ± 0.26	0.13 ± 0.01	0.19 ± 0.04	1.54 ± 0.22
20% BUPA	1.61 ± 0.12	0.15 ± 0.01	0.20 ± 0.07	0.95 ± 0.12
10% BUPA	1.66 ± 0.26	0.14 ± 0.01	0.21 ± 0.05	1.03 ± 0.37
0% BUPA	1.51 ± 0.11	0.15 ± 0.01	–	0.60 ± 0.13

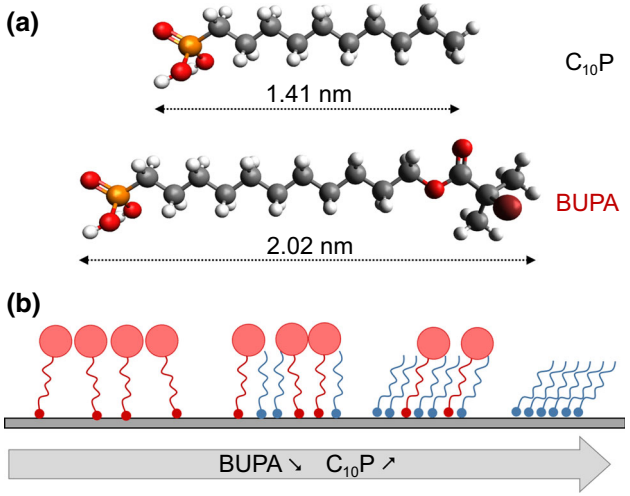

Fig. 4: Model structures of C_{10}P and BUPA (a) and schematic representation of BUPA/C_{10}P coating thickness (based on XPS results) (b)

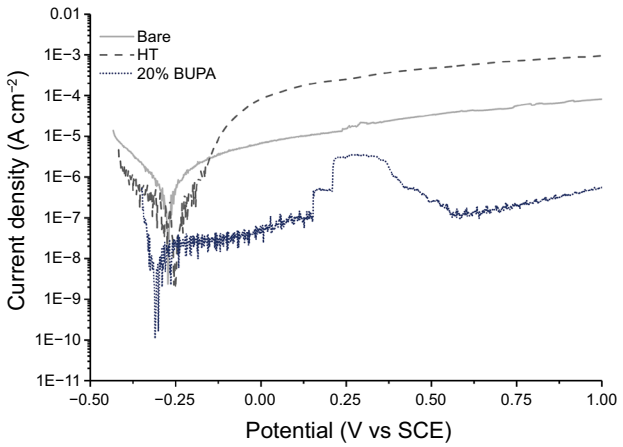

Fig. 5: Representative polarization curves for bare NiTi, HT-NiTi, and representative BUPA/C_{10}P-NiTi (20/80) in 0.5 M NaCl at a scan rate of 1 mV s^{-1}

The approximated thickness of BUPA layer (1.93 ± 0.38 nm) is consistent with the simulated value of 2.02 nm (Fig. 4a), whereas the estimated thickness of C_{10}P layer is underestimated from a theoretical value of 1.41 nm to 0.60 ± 0.13 nm. This difference could result from a tilted denser organization of the C_{10}P layer. The coating thickness decreases with the incorporation of C_{10}P (Table 1), which also attests to the formation of a tilted denser layer as shown in Fig. 4b.

Electrochemical evaluation of modified NiTi is compared to HT-NiTi on the basis of three methods (LSV, CV, and SECM). LSV results (Fig. 5 and Table 2—Supporting Information Figure S1) indicate a strong improvement of the corrosion resistance of BUPA/C_{10}P-NiTi with the decrease in BUPA amount, e.g., corrosion current density (j_{corr}) decreases from 95.1 nA cm^{-2} to 9.4 nA cm^{-2} for 20% of BUPA. This is once again in accordance with the formation of a denser and more organized layer due to higher amount of C_{10}P within the layer.

As expected, the use of high C_{10}P amount leads to the formation of more resistant layers. Among all the conditions, the layers made of 20 and 50% of BUPA exhibit the best inhibition efficiencies (IE) with respective values of 98.7% and 98.9%, hence the best resistance against corrosion.

Cyclic voltammetry (CV) (Fig. 6 and Table 2—Supporting information Figure S2) confirms the protective efficiency due to BUPA and C_{10}P grafting, as well as the reinforcement of the TiO_2 external layer.

For bare NiTi substrate, the first cycle reveals two anodic peaks at 200 and 500 mV vs SCE, respectively, assigned to Ti^{n+} and Ni^{2+} oxidations, but only one cathodic peak assigned to Ni^{3+} reduction. On the second cycle, only nickel oxidation and reduction

Table 2: Values of E_{corr}, j_{corr}, IE, BF, and k_{ct} for bare NiTi, HT-NiTi, and BUPA/C_{10}P-NiTi (in various ratios) (obtained by LSV, CV, and SECM)

Sample	E_{corr} (mV vs SCE)	j_{corr} (nA cm^{-2})	IE (%)	BF (%)	k_{ct} (μm s^{-1})
Bare	− 294 ± 65	869.2 ± 288.5	–	–	16.0 ± 1.3
NiTi-HT	− 266 ± 22	103.6 ± 22.2	88.1 ± 2.6	46.4 ± 11.0	10.8 ± 1.1
100% BUPA	− 262 ± 34	95.1 ± 28.8	89.1 ± 3.3	72.3 ± 5.0	1.8 ± 1.6
90% BUPA	− 233 ± 70	29.2 ± 21.1	96.6 ± 2.4	96.3 ± 1.9	1.2 ± 0.1
80% BUPA	− 193 ± 45	31.2 ± 17.1	96.4 ± 2.0	84.4 ± 6.4	0.5 ± 0.3
70% BUPA	− 217 ± 24	35.7 ± 27.2	95.9 ± 3.1	88.0 ± 16.7	2.1 ± 0.6
60% BUPA	− 289 ± 19	72.3 ± 3.8	91.7 ± 0.4	76.8 ± 23.1	0.4 ± 0.2
50% BUPA	− 194 ± 86	11.1 ± 10.4	98.7 ± 1.2	98.2 ± 0.3	1.8 ± 0.2
40% BUPA	− 296 ± 13	109.4 ± 41.2	87.4 ± 4.7	86.0 ± 8.1	0.9 ± 0.2
30% BUPA	− 160 ± 96	32.9 ± 22.2	96.2 ± 2.6	88.2 ± 10.5	1.0 ± 0.2
20% BUPA	− 314 ± 41	9.4 ± 6.4	98.9 ± 0.7	93.9 ± 6.6	0.6 ± 0.1
10% BUPA	− 252 ± 56	82.7 ± 55.6	90.5 ± 6.4	93.7 ± 2.1	0.7 ± 0.1
0% BUPA	− 256 ± 29	59.0 ± 38.9	93.5 ± 4.5	97.1 ± 2.3	0.4 ± 0.2

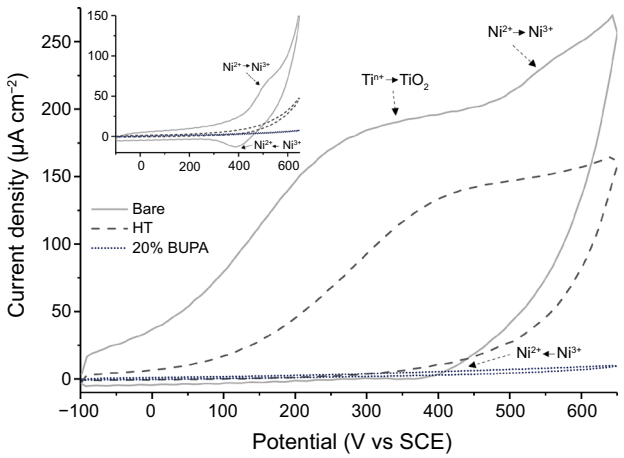

Fig. 6: Representative first (main) and second (inset) cycles of the voltammograms for bare NiTi, HT-NiTi, and BUPA/C_{10}P-NiTi (20/80) in 0.1 M NaOH at a scan rate of 20 mV s^{-1}

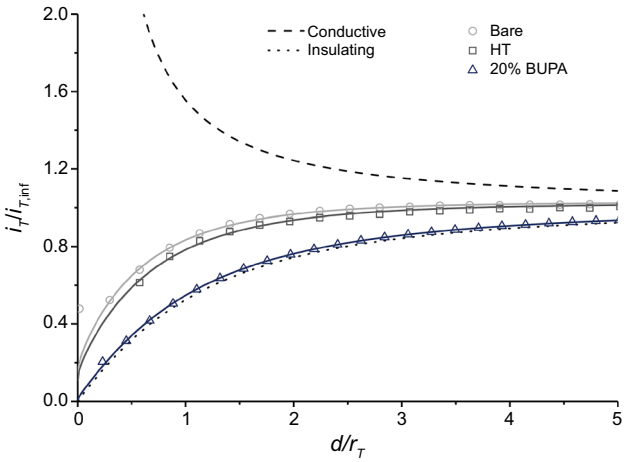

Fig. 7: Representative normalized SECM FB approach curves for bare NiTi (k_{ct} = 15.3), HT-NiTi (k_{ct} = 11.2), representative BUPA/C_{10}P-NiTi (20/80) (k_{ct} = 0.6) in 1 mM FeMeOH/0.1 M KNO_3. The tip was set at 0.4 V vs Ag|AgCl and moved at a scan rate of 1 μm s^{-1}. The symbols correspond to the experimental curves and the solid lines to the SECM theory[61,62]

peaks are still present due to the irreversible passivation of the electrode via the titanium oxide layer. For HT-NiTi, only the oxidation peak of Ti^{n+} can be observed on the first cycle and no more Ni reactions, even during the second cycle. This confirms the efficiency of the hydrothermal treatment on the reinforcement of TiO_2 layer and on the prevention of Ni^{x+} release. Once electroassisted grafting of BUPA/C_{10}P is performed on HT-NiTi, their CV analysis does not show any electrochemical activity, thus confirming the protective efficiency of the grafted phosphonic derivatives. As expected, the increase in C_{10}P concentration within the layer leads to the formation of more blocking layers. In line with the conclusions made from LSV results, BUPA/C_{10}P ratios of 50/50 and 20/80 exhibit the best blocking factors and thus the best protection of the substrate.

SECM is used to assess the charge transfer process occurring at bare NiTi, HT-NiTi, and BUPA/C_{10}P-NiTi electrodes during the reduction of $FcMeOH^+$. Figure 7 and Figure S3 (Supporting information) show the normalized approach curves in FB mode. The curves are fitted on general analytical expressions given for first-order heterogeneous finite kinetics[61,62] at the sample surface with respect to the $FcMeOH^+$ generated at the tip surface.

The apparent charge transfer rate constants (k_{ct}, Table 2) attests to the regeneration rate of FcMeOH by the NiTi samples evolving through the modification steps. The obtained values of k_{ct} are in line with the results presented for CV. Indeed, the hydrothermal

passivation of NiTi leads to the formation of a slightly more protective oxide layer, as attested by a k_{ct} down from 16.0 to 10.8 μm s^{-1}. This phenomenon is amplified by the additional presence of BUPA/C_{10}P monolayers, with k_{ct} ranging from 0.4 to 10.5 μm s^{-1}. Among the assessed BUPA/C_{10}P ratios, the best results are obtained for the coatings with 0, 60, 80, and 20% BUPA with respective k_{ct} of 0.4, 0.4, 0.5, or 0.6 μm s^{-1}.

From these results, the optimum BUPA/C_{10}P layer (high P/NiTi, Br/NiTi, BF, IE, k_{ct}, and reproducibility) is prepared from 20% of BUPA and 80% of C_{10}P. This molecular ratio will be used for all the upcoming functionalization.

Surface-initiated atom transfer radical polymerization of 2-methacryloyloxyethyl phosphorylcholine on BUPA/C_{10}P-NiTi

In this section, SI-ATRP of MPC is performed on the BUPA/C_{10}P-NiTi (modified in the optimum conditions determined above (i.e., E = 1.2 V vs SCE, t = 5mn, BUPA/C_{10}P = 20/80) for 1, 3, and 6 h (PMPC-NiTi).

The modified surfaces are first characterized using water contact angle (Fig. 8). More hydrophilic surfaces (θ_w = 45°) are obtained for PMPC-NiTi compared to BUPA/C_{10}P-NiTi (78.9°) which confirms, considering the hydrophilic nature of the MPC, the formation and the grafting of the polymer.

Figure 9 shows the PM-IRRAS spectra. For PMPC-NiTi coatings, absorption bands in agreement with the structure of the molecules appear at 1721, 1486, 1255–1279, 1170, 1125, 1092, and 1054 cm^{-1}, respectively, assigned to $C{=}O_{stretch}$ (ester), $C{-}O{-}C_{wag}$, $C{-}O_{asym\ stretch}$ (ester), $C{-}O_{sym\ stretch}$ (ester), $C{-}N_{stretch}$, $C{-}O_{stretch}$ (alcohol), and $P{-}O_{stretch}$. An increased signal is noticed, especially after 6 h of polymerization, which confirms the presence of a PMPC film on NiTi surface.

XPS analyses confirm the formation of PMPC. Figure 10 presents C1s and N1s core-level spectra for PMPC-NiTi and BUPA/C_{10}P-NiTi. As expected, C1s and N1s peaks are more intense after SI-ATRP of MPC and present different general shapes compared to the initial BUPA/C_{10}P-NiTi. The C1s core-level spectra (Fig. 10-left) present four components centered at energies of 285.0, 285.7, 286.5, and 289.1 eV, respectively, attributed to carbon atoms involved in C–H/C–C, C–N, C–O/C–P, and O–C=O bonds present in BUPA, C_{10}P, PMPC, and Me_6TREN. The peak at 283.3 eV (*) assigned previously to an artifact from the spectrometer is still visible.

The N1s core-level spectra (Fig. 10-right) present two components centered at energies of 400.3 eV and 403.5 eV, respectively, attributed to nitrogen atoms characteristic of the amine function of the Me_6TREN and of the ammonium present in PMPC. These confirm the efficiency of SI-ATRP of MPC on BUPA/C_{10}P (20/80) layer but also point out the presence of residues of the catalyst (complexed by Me_6TREN) trapped in the coating.

SEM images (Fig. 11) highlight the differences of modified NiTi morphologies as a function of the polymerization time. Within short polymerization time (1 h), the surface is highly inhomogeneous and shows a high density of polymer aggregates. After 3 h, the coating starts to be more homogenous but uncovered NiTi domains are still visible. However, the formation of PMPC film for 6 h leads to a good coverage with a quite uniform distribution of small aggregation spots probably resulting from nonuniform PMPC growth.

The increase in the hydrophylicity of PMPC-NiTi and the time-dependent homogeneity of the surface induced differences in the electrochemical properties which are shown in the LSV curves (Fig. 12) and SECM images (Fig. 13).

For the substrate modified for 1 h, j_{corr} changes from 9.4 nA cm^{-2} (BUPA/C10P-NiTi) to a value of 92.5 nA cm^{-2} as well as less negative E_{corr} (from − 314 to − 82 mV vs SCE) due to the high hydrophilicity and inhomogeneity of the PMPC layer. For higher SI-ATRP times, j_{corr} values are 12.0 nA cm^{-2} and 17.8 nA

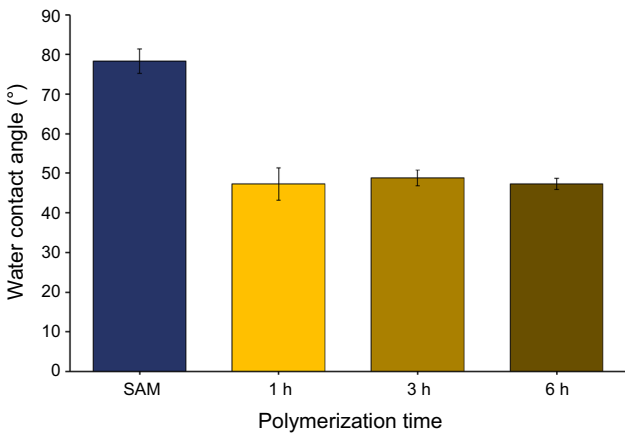

Fig. 8: Water contact angles for BUPA/C_{10}P NiTi (20/80) and PMPC-NiTi prepared for 1, 3, or 6 h

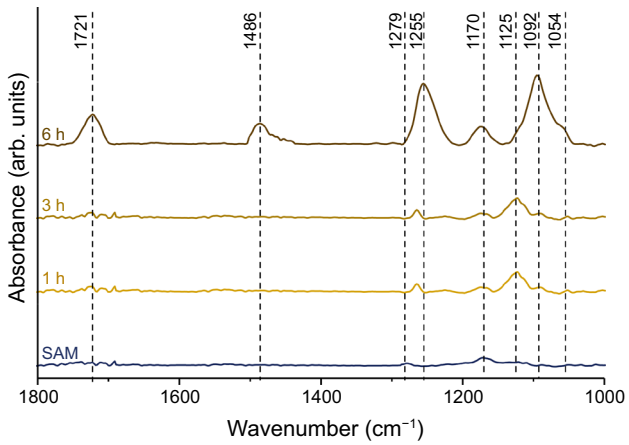

Fig. 9: PM-IRRAS for BUPA/C_{10}P NiTi (20/80) and PMPC-NiTi prepared for 1, 3, or 6 h

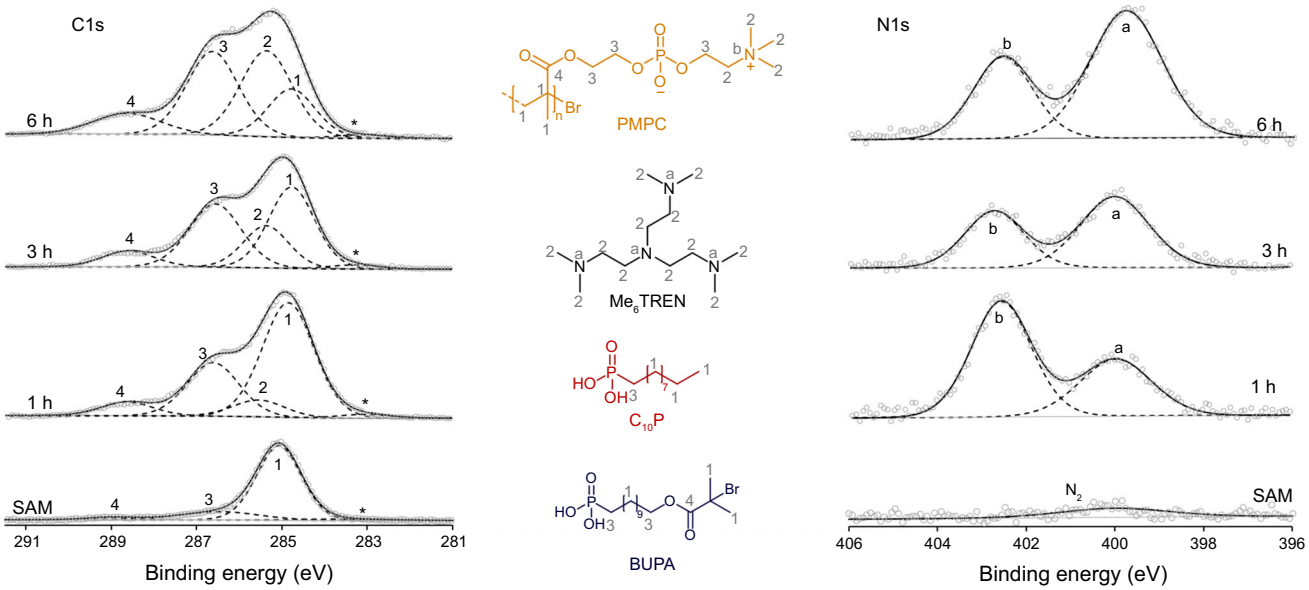

Fig. 10: XPS general shape of core spectra for C1s and N1s components obtained for BUPA/C_{10}P NiTi (20/80) and PMPC-NiTi prepared for 1, 3, or 6 h

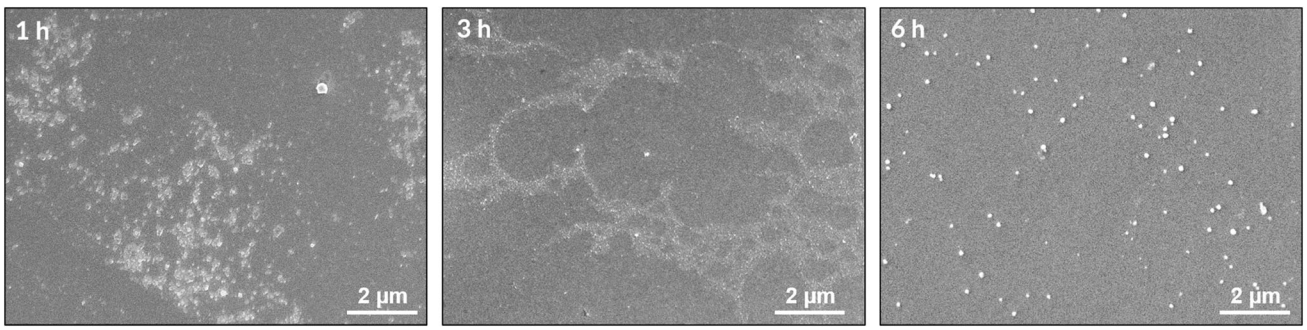

Fig. 11: SEM images of PMPC-NiTi prepared for 1, 3, or 6 h

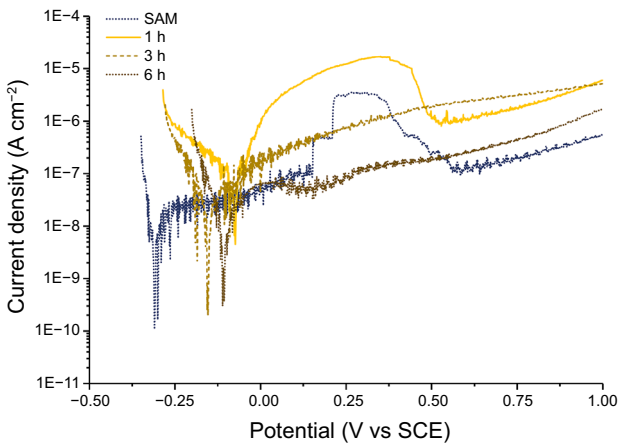

Fig. 12: Polarization curves for BUPA/C_{10}P NiTi (20/80) and PMPC-NiTi prepared for 1, 3, or 6 h (obtained in 0.5 M NaCl at a scan rate of 1 mV s^{-1})

cm^{-2} for 3 h and 6 h, respectively. E_{corr} values remain in the same range with values of − 110 and − 153 mV vs SCE.

Nevertheless, compared to HT-NiTi ($j_{corr} \sim 103.6$ nA cm^{-2}, IE ∼ 88.1, and $E_{corr} \sim -266$ mV vs SCE), the corrosion current and inhibition efficiency still indicate an improvements of the corrosion inhibition properties.

Representative SECM mapping images collected in FB mode are presented in Fig. 13. Those point out the surface uniformity and the passivating behavior of BUPA/C_{10}P SAM (Fig. 13—upper left). However, once SI-ATRP of MPC occurred, the average measured current increases up from ∼ 0.2 to ∼ 0.4 nA with a slightly less homogeneous behavior. These results are in line with the previous observations made from SEM pictures (Fig. 11) and LSV curves (Fig. 12). The increased PMPC thickness induces a heterogeneous electroactivity, especially for the 6-h polymerization, where several high current spots are noticeable. The increased electroreactivity is in accordance with the

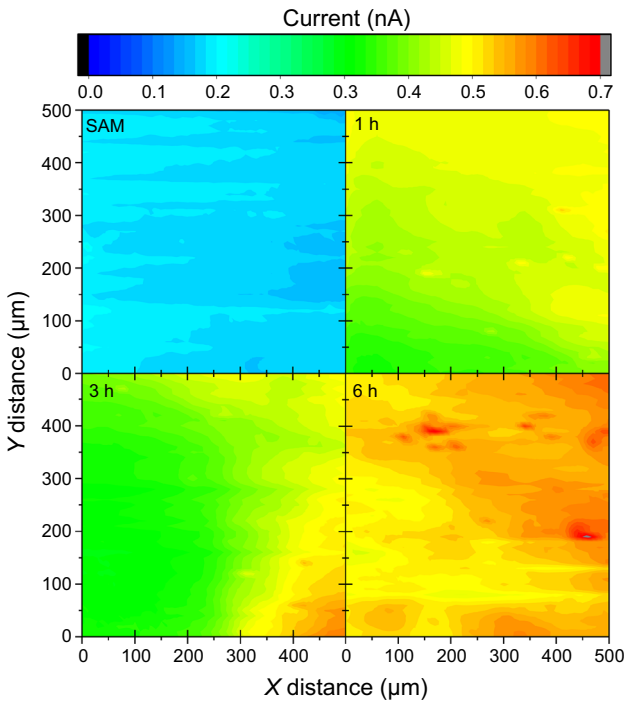

Fig. 13: Normalized SECM FB mapping for BUPA/C_{10}P NiTi (20/80) and PMPC-NiTi prepared for 1, 3, or 6 h (obtained in 1 mM FeMeOH/0.1 M KNO_3)

hydrophilic behavior of PMPC coatings and thus the interactions between the coating and the redox probe, thus resulting in an intercalation of the probe inside the organic layer. In 2010, Matrab et al. investigated to transport and reactivity within PGMA polymer brushes made by SI-ATRP and proved the permeability of such methacrylate-based polymer once solvated in aqueous media.

Conclusions

In this work, the electroassisted grafting of BUPA/C_{10}P mixed monolayers in various ratios has been achieved to improve NiTi corrosion resistance.

First, the successful surface modifications have been attested by WCA, PM-IRRAS, and XPS results, and it has been proven that the substitution of some BUPA molecules by C_{10}P (a smaller and less hindered molecule) improves the anticorrosion properties of Nitinol. Among all the tested conditions, the most protective and efficient layer (high blocking factor, high inhibition efficiency, low charge transfer constant k_{ct}) is obtained for a composition of 20% BUPA and 80% C_{10}P.

Second, the surface-initiated ATRP of MPC has been achieved on the so-formed initiating layer for 1, 3, or 6 h. SEM images and SECM measurements evidenced the nonuniformity of the PMPC coatings for time lower than 6 h.

This work opens the prospect of biocompatible polymer growth and tuning on Nitinol substrate modified by electrografted phosphonic-made ATRP initiators. Nevertheless, the structure of this system still requires some improvements with the prospect of a further biomedical application, which is being evaluated in simulated body fluids.

Acknowledgments B. A. thanks UNamur and UMONS for the joint PhD grant. B. A., L. M., and P. D. acknowledge the Belgian Program on Interuniversity Attraction Poles initiated by the Belgian State, the Prime Minister's office (P7/05). CIRMAP is grateful to the "Belgian Federal Government Office Policy of Science (SSTC)" for general support in the frame of the PAI-7/05, the European Commission and the Wallonia Region (FEDER Program), and OPTI^{2}MAT program of excellence.

References

1. Duerig, T, Pelton, A, Stöckel, D, "An Overview of Nitinol Medical Applications." *Mater. Sci. Eng. A*, **273–275** 149–160 (1999)
2. Elahinia, MH, Hashemi, M, Tabesh, M, Bhaduri, SB, "Manufacturing and Processing of NiTi Implants: A Review." *Prog. Mater. Sci.*, **57** (5) 911–946 (2012)
3. Shabalovskaya, SA, "Surface, Corrosion and Biocompatibility Aspects of Nitinol as an Implant Material." *Biomed. Mater. Eng.*, **12** (1) 69–109 (2002)
4. Centre d'Animation Régional en Matériaux Avancés (C.A.R.M.A.). *Alliages à Mémoire de Forme* (2001).
5. Mantovani, D, "Shape Memory Alloys: Properties and Biomedical Applications." *JOM*, **52** (10) 36–44 (2000)
6. Mohd Jani, J, Leary, M, Subic, A, Gibson, MA, "A Review of Shape Memory Alloy Research, Applications and Opportunities." *Mater. Des.*, **56** 1078–1113 (2014)
7. Duerig, TW, Melton, KN, Stöckel, D, *Engineering Aspects of Shape Memory Alloys*. Butterwort, London (1990)
8. Airoldi, G, Riva, G, Vanelli, M, "Superelasticity and Shape Memory Effect in NiTi Orthodontic Wires." *J. Phys. IV*, **05** (C8) 1205–1210 (1995)
9. Laster, Z, MacBean, AD, Ayliffe, PR, Newlands, LC, "Fixation of a Frontozygomatic Fracture with a Shape-Memory Staple." *Br. J. Oral Maxillofac. Surg.*, **39** (4) 324–325 (2001)
10. Luebke, N, Brantley, W, Alapati, S, Mitchell, J, Lausten, L, Daehn, G, "Bending Fatigue Study of Nickel-Titanium Gates Glidden Drills." *J. Endod.*, **31** (7) 523–525 (2005)
11. Shabalovskaya, SA, Rondelli, GC, Undisz, AL, Anderegg, JW, Burleigh, TD, Rettenmayr, ME, "The Electrochemical Characteristics of Native Nitinol Surfaces." *Biomaterials*, **30** (22) 3662–3671 (2009)
12. Shabalovskaya, SA, Tian, H, Anderegg, JW, Schryvers, DU, Carroll, WU, Van Humbeeck, J, "The Influence of Surface Oxides on the Distribution and Release of Nickel from Nitinol Wires." *Biomaterials*, **30** (4) 468–477 (2009)

13. Figueira, N, Silva, TM, Carmezim, MJ, Fernandes, JCS, ''Corrosion Behaviour of NiTi Alloy.'' *Electrochim. Acta*, **54** (3) 921–926 (2009)
14. Milošev, I, Kapun, B, ''The Corrosion Resistance of Nitinol Alloy in Simulated Physiological Solutions: Part 1: The Effect of Surface Preparation.'' *Mater. Sci. Eng. C*, **32** (5) 1087–1096 (2012)
15. Lü, X, Bao, X, Huang, Y, Qu, Y, Lu, H, Lu, Z, ''Mechanisms of Cytotoxicity of Nickel Ions Based on Gene Expression Profiles.'' *Biomaterials*, **30** (2) 141–148 (2009)
16. Lee, J, Son, Y, Pratheeshkumar, P, Shi, X, ''Oxidative Stress and Metal Carcinogenesis.'' *Free Radic. Biol. Med.*, **53** (4) 742–757 (2012)
17. Yang, J, Wang, J, Tong, S, ''Surface Properties of Bio-Implant Nitinol Modified by ECR Cold Plasma.'' *Mater. Sci. Technol.*, **20** (November) 1427–1431 (2004)
18. Shen, Y, Wang, G, Chen, L, Li, H, Yu, P, Bai, M, Zhang, Q, Lee, J, Yu, Q, ''Investigation of Surface Endothelialization on Biomedical Nitinol (NiTi) Alloy: Effects of Surface Micropatterning Combined with Plasma Nanocoatings.'' *Acta Biomater.*, **5** (9) 3593–3604 (2009)
19. Siu, HT, Man, HC, ''Fabrication of Bioactive Titania Coating on Nitinol by Plasma Electrolytic Oxidation.'' *Appl. Surf. Sci.*, **274** 181–187 (2013)
20. Lahann, J, Klee, D, Thelen, H, Bienert, H, Vorwerk, D, Höcker, H, ''Improvement of Haemocompatibility of Metallic Stents by Polymer Coating.'' *J. Mater. Sci. Mater. Med.*, **10** (7) 443–448 (1999)
21. Catledge, SA, Thomas, V, Vohra, YK, ''Effect of Surface Oxides and Intermetallics on Nanostructured Diamond Coating of Nitinol.'' *Curr. Nanosci.*, **2** (1) 9–12 (2006)
22. Pérez, LM, Gracia-Villa, L, Puértolas, JA, Arruebo, M, Irusta, S, Santamaría, J, ''Effect of Nitinol Surface Treatments on Its Physico-Chemical Properties.'' *J. Biomed. Mater. Res. B. Appl. Biomater.*, **91** (1) 337–347 (2009)
23. Devillers, S, Barthélémy, B, Delhalle, J, Mekhalif, Z, ''Induction Heating Vs Conventional Heating for the Hydrothermal Treatment of Nitinol and Its Subsequent 2-(Methacryloyloxy)Ethyl 2-(Trimethylammonio)Ethyl Phosphate Coating by Surface-Initiated Atom Transfer Radical Polymerization.'' *ACS Appl. Mater. Interfaces*, **3** (10) 4059–4066 (2011)
24. Quiñones, R, Gawalt, ES, ''Study of the Formation of Self-Assembled Monolayers on Nitinol.'' *Langmuir*, **23** (20) 10123–10130 (2007)
25. Petrovic, Z, Katic, J, Metikos-Hukovic, M, Dadafarin, H, Omanovic, S, ''Modification of a Nitinol Surface by Phosphonate Self-Assembled Monolayers.'' *J. Electrochem. Soc.*, **158** (10) F159–F165 (2011)
26. Maho, A, Kanoufi, F, Combellas, C, Delhalle, J, Mekhalif, Z, ''Electrochemical Investigation of Nitinol/Tantalum Hybrid Surfaces Modified by Alkylphosphonic Self-Assembled Monolayers.'' *Electrochim. Acta*, **116** 78–88 (2014)
27. Quiñones, R, Gawalt, ES, ''Polystyrene Formation on Monolayer-Modified Nitinol Effectively Controls Corrosion.'' *Langmuir*, **24** (19) 10858–10864 (2008)
28. Marcinko, S, Fadeev, AY, ''Hydrolytic Stability of Organic Monolayers Supported on TiO_2 and ZrO_2.'' *Langmuir*, **20** (3) 2270–2273 (2004)
29. Bhure, R, Mahapatro, A, Bonner, C, Abdel-Fattah, TM, ''In Vitro Stability Study of Organophosphonic Self Assembled Monolayers (SAMs) on Cobalt Chromium (Co-Cr) Alloy.'' *Mater. Sci. Eng. C*, **33** (4) 2050–2058 (2013)
30. Mahapatro, A, Matos Negrón, TD, Nguyen, A, ''Spectroscopic Evaluations of Interfacial Oxidative Stability of Phosphonic Nanocoatings on Magnesium.'' *J. Spectrosc.*, **2015** 1–8 (2015)
31. Guerrero, G, Alauzun, JG, Granier, M, Laurencin, D, Mutin, PH, ''Phosphonate Coupling Molecules for the Control of Surface/Interface Properties and the Synthesis of Nanomaterials.'' *Dalt. Trans.*, **42** (35) 12569 (2013)
32. Mani, G, Johnson, DM, Marton, D, Dougherty, VL, Feldman, MD, Patel, D, Ayon, AA, Agrawal, CM, ''Stability of Self-Assembled Monolayers on Titanium and Gold.'' *Langmuir*, **24** (13) 6774–6784 (2008)
33. Ishizaki, T, Okido, M, Masuda, Y, Saito, N, Sakamoto, M, ''Corrosion Resistant Performances of Alkanoic and Phosphonic Acids Derived Self-Assembled Monolayers on Magnesium Alloy AZ31 by Vapor-Phase Method.'' *Langmuir*, **27** (10) 6009–6017 (2011)
34. Abohalkuma, T, Telegdi, J, ''Corrosion Protection of Carbon Steel by Special Phosphonic Acid Nano-Layers.'' *Mater. Corros.*, **12** 1382–1390 (2015)
35. Quiñones, R, Raman, A, Gawalt, ES, ''Functionalization of Nickel Oxide Using Alkylphosphonic Acid Self-Assembled Monolayers.'' *Thin Solid Films*, **516** (23) 8774–8781 (2008)
36. Devillers, S, Lemineur, JF, Dilimon, VS, Barthélémy, B, Delhalle, J, Mekhalif, Z, ''Polyelectrolyte Multilayer Deposition on Nickel Modified with Self-Assembled Monolayers of Organophosphonic Acids for Biomaterials: Electrochemical and Spectroscopic Evaluation.'' *J. Phys. Chem. C*, **116** (36) 19252–19261 (2012)
37. Guerrero, G, Alauzun, JG, Granier, M, Laurencin, D, Mutin, PH, ''Phosphonate Coupling Molecules for the Control of Surface/Interface Properties and the Synthesis of Nanomaterials.'' *Dalt. Trans.*, **42** (35) 12569 (2013)
38. Liu, P, Huang, T, Liu, P, Shi, S, Chen, Q, Li, L, Shen, J, ''Zwitterionic Modification of Polyurethane Membranes for Enhancing the Anti-Fouling Property.'' *J. Colloid Interface Sci.*, **480** 91–101 (2016)
39. Rodriguez-Emmenegger, C, Hasan, E, Pop-Georgievski, O, Houska, M, Brynda, E, Alles, AB, ''Controlled/Living Surface-Initiated ATRP of Antifouling Polymer Brushes from Gold in PBS and Blood Sera as a Model Study for Polymer Modifications in Complex Biological Media.'' *Macromol. Biosci.*, **12** (4) 525–532 (2012)
40. Shahsavan, H, Quinn, J, D'Eon, J, Zhao, B, ''Surface Modification of Polydimethylsiloxane Elastomer for Stable Hydrophilicity, Optical Transparency and Film Lubrication.'' *Colloids Surfaces A Physicochem. Eng. Asp.*, **482** 267–275 (2015)
41. Zhang, J, Xiao, S, Shen, M, Sun, L, Chen, F, Fan, P, Zhong, M, Yang, J, ''Aqueous Lubrication of Poly(N-Hydroxyethyl Acrylamide) Brushes: A Strategy for Their Enhanced Load Bearing Capacity and Wear Resistance.'' *RSC Adv.*, **6** (26) 21961–21968 (2016)
42. Lilge, I, Schönherr, H, ''Synthesis and Characterization of Well-Defined Ligand-Terminated Block Copolymer Brushes for Multifunctional Biointerfaces.'' *Polymer (Guildf)*, **98** 409–420 (2016)
43. Wu, T, Tan, L, Cheng, N, Yan, Q, Zhang, Y-F, Liu, C-J, Shi, B, ''PNIPAAM Modified Mesoporous Hydroxyapatite for Sustained Osteogenic Drug Release and Promoting Cell Attachment.'' *Mater. Sci. Eng. C*, **62** 888–896 (2016)
44. Lilge, I, Jiang, S, Wesner, D, Schönherr, H, ''The Effect of Size and Geometry of Poly(Acrylamide) Brush-Based Micropatterns on the Behavior of Cells.'' *ACS Appl. Mater. Interfaces*, **8** (36) 23591–23603 (2016)
45. Ezzat, M, Huang, C-J, ''Zwitterionic Polymer Brush Coatings with Excellent Anti-Fog and Anti-Frost Properties.'' *RSC Adv.*, **6** (66) 61695–61702 (2016)

46. Schuh, C, Santer, S, Prucker, O, Rühe, J, ''Polymer Brushes with Nanometer-Scale Gradients.'' *Adv. Mater.*, **21** (46) 4706–4710 (2009)
47. Barthélémy, B, Maheux, S, Devillers, S, Kanoufi, F, Combellas, C, Delhalle, J, Mekhalif, Z, ''Synergistic Effect on Corrosion Resistance of Phynox Substrates Grafted with Surface-Initiated ATRP (Co)Polymerization of 2-Methacryloyloxyethyl Phosphorylcholine (MPC) and 2-Hydroxyethyl Methacrylate (HEMA).'' *ACS Appl. Mater. Interfaces*, **6** (13) 10060–10071 (2014)
48. Luo, Y-R, *Comprehensive Handbook of Chemical Bond Energies*. CRC Press, Boca Raton (2007)
49. Arrotin, B, Delhalle, J, Dubois, P, Mespouille, L, Mekhalif, Z, ''Electroassisted Functionalization of Nitinol Surface, a Powerful Strategy for Polymer Coating through Controlled Radical Surface Initiation.'' *Langmuir*, **33** (12) 2977–2985 (2017)
50. Metoki, N, Liu, L, Beilis, E, Eliaz, N, Mandler, D, ''Preparation and Characterization of Alkylphosphonic Acid Self-Assembled Monolayers on Titanium Alloy by Chemisorption and Electrochemical Deposition.'' *Langmuir*, **30** (23) 6791–6799 (2014)
51. Vanhooland, A, Devillers, S, Issakova, T, Michaux, C, Delhalle, J, Mekhalif, Z, ''Electroassisted Auto-Assembly of Alkylphosphonic Acids Monolayers on Nitinol.'' *J. Electrochem. Soc.*, **163** (10) G173–G177 (2016)
52. Gupta, RK, Singh, RA, ''Inhibition of Corrosion by Poly(N-Hexadecylaniline)/Docosanol Mixed Langmuir-Blodgett Films on Copper in Sea Water.'' *Mater. Chem. Phys.*, **97** (2–3) 226–229 (2006)
53. Li, C, Li, L, Wang, C, ''Study of the Inhibitive Effect of Mixed Self-Assembled Monolayers on Copper with SECM.'' *Electrochim. Acta*, **115** 531–536 (2014)
54. Barthélémy, B, Kanoufi, F, Combellas, C, Delhalle, J, Mekhalif, Z, ''Phynox Improved Corrosion Resistance with MPC Initiated from Mixed Monolayers of Phosphonic Acids.'' *J. Electrochem. Soc.*, **161** (12) C1–C6 (2014)
55. Sae-ung, P, Kolewe, KW, Bai, Y, Rice, EW, Schiffman, JD, Emrick, T, Hoven, VP, ''Antifouling Stripes Prepared from Clickable Zwitterionic Copolymers.'' *Langmuir*, **33** (28) 7028–7035 (2017)
56. Chastain, J (ed.) *Handbook of X-Ray Photoelectron Spectroscopy*. Perkin Elmer Corporation, Waltham (1992)
57. Cumpson, PJ, Seah, MP, ''Elastic Scattering Corrections in AES and XPS. II. Estimating Attenuation Lengths and Conditions Required for Their Valid Use in Overlayer/Substrate Experiments.'' *Surf. Interface Anal.*, **25** (6) 430–446 (1997)
58. Chamoulaud, G, Belanger, D, ''Spontaneous Derivatization of a Copper Electrode with in Situ Generated Diazonium Cations in Aprotic and Aqueous Media.'' *J. Phys. Chem. C*, **111** (20) 7501–7507 (2007)
59. Maho, A, Kanoufi, F, Combellas, C, Delhalle, J, Mekhalif, Z, ''Electrochemical Investigation of Nitinol/Tantalum Hybrid Surfaces Modified by Alkylphosphonic Self-Assembled Monolayers.'' *Electrochim. Acta*, **116** 78–88 (2014)
60. Socrates, G, *Infrared and Raman Characteristic Group Frequencies: Tables and Charts*, Vol. Third. Wiley, London (2004)
61. Wei, C, Bard, AJ, Mirkin, MV, ''Scanning Electrochemical Microscopy. 31. Application of SECM to the Study of Charge Transfer Processes at the Liquid/Liquid Interface.'' *J. Phys. Chem.*, **99** (43) 16033–16042 (1995)
62. Cannes, C, Kanoufi, F, Bard, AJ, ''Cyclic Voltammetry and Scanning Electrochemical Microscopy of Ferrocenemethanol at Monolayer and Bilayer-Modified Gold Electrodes.'' *J. Electroanal. Chem.*, **547** (1) 83–91 (2003)